Chinese Chemical Letters 33 (2022) 3849–3852

Contents lists available at ScienceDirect

Chinese Chemical Letters

journal homepage: www.elsevier.com/locate/cclet

Porous covalent organic frameworks-improved solid phase microextraction ambient mass spectrometry for ultrasensitive analysis of tetrabromobisphenol-A analogs

Wei Gao[a,b], Min Li[b], Yun Fa[b,*], Zongshan Zhao[b,c,**], Yaqi Cai[d], Xiangfeng Liang[b,e], Yongliang Yu[a,*], Guibin Jiang[d]

[a] Research Center for Analytical Sciences, Department of Chemistry, College of Sciences, Northeastern University, Shenyang 110819, China
[b] CAS Key Laboratory of Biobased Materials, Qingdao Institute of Bioenergy and Bioprocess Technology, Chinese Academy of Sciences, Qingdao 266101, China
[c] College of Environmental Science and Engineering, Qingdao University, Qingdao 266071, China
[d] State Key Laboratory of Environmental Chemistry and Ecotoxicology, Research Center for Eco-Environmental Sciences, Chinese Academy of Sciences, Beijing 100085, China
[e] Innovation Academy for Green Manufacture, Chinese Academy of Sciences, Beijing 100190, China

ARTICLE INFO

Article history:
Received 25 June 2021
Revised 23 August 2021
Accepted 13 October 2021
Available online 21 October 2021

Keywords:
Environmental analysis
Covalent organic frameworks
Solid phase microextraction
Ambient mass spectrometry
TBBPA analogs

ABSTRACT

Owing to frequent environmental monitoring of tetrabromobisphenol-A (TBBPA) analogs and their potential ecotoxicological effects on organisms, analysis of trace levels of TBBPA analogs with more non-polar and less water-soluble characteristics is of great significance for studying their environmental behaviors and toxic effects. Herein, a fast and sensitive technique is developed for directly detecting aqueous TBBPA analogs, including TBBPA mono(allyl ether) (TBBPA-MAE), TBBPA mono(2,3-dibromopropyl ether) (TBBPA-MDBPE), TBBPA mono(2-hydroxyethyl ether) (TBBPA-MHEE) and TBBPA mono(glycidyl ether) (TBBPA-MGE), by combining solid phase microextraction (SPME) based on porous covalent organic frameworks (Porous-COFs) with constant flow desorption ionization-mass spectrometry (CFDI-MS). As chromatographic separation is replaced by constant flow desorption, each sample can be analyzed within 7 min. The hierarchical porous structures (microporous, mesoporous and macroporous) of COFs lead to the enhanced mass transfer and the easier accessibility of active sites to TBBPA analogs, so that the extraction efficiency is 2.3–3.6 times higher than pure microporous COFs, and far superior to commercial coatings. The detection limit and quantification limit of this method are 0.1–1 and 0.4–3.2 ng/L, respectively. Ultratrace levels of TBBPA analogs from 5.0 ng/L to 66 ng/L have been successfully detected in river and sea water samples, showing great potential for subsequent studies of their environmental behaviors and toxicological effects

Tetrabromobisphenol-A (TBBPA) and its analogs, as one of the most widely used brominated flame retardants (BFRs), have attracted much attention due to their extensive use, distribution and unfavorable influence on environmental safety, biological life and human health [1,2]. TBBPA analogs, *e.g.*, TBBPA mono(allyl ether) (TBBPA-MAE), TBBPA mono(2,3-dibromopropyl ether) (TBBPA-MDBPE), TBBPA mono(2-hydroxyethyl ether) (TBBPA-MHEE) and TBBPA mono(glycidyl ether) (TBBPA-MGE), have similar physicochemical properties to TBBPA, presenting potential environmental and health risks [3,4]. Different from TBBPA, TBBPA analogs are more non-polar and less water soluble. Analysis of trace levels of TBBPA analogs is highly demanded in order to study their distribution, transportation, transformation and ecotoxicological effects [5,6]. Hence, sample preparation involving extraction and purification is often necessary prior to instrumental analysis. Solid phase microextraction (SPME), as a sample pretreatment technology integrating the functions of sampling, separation and enrichment, can fast extract, enrich and purify the analyte from complex environmental matrix [7–9]. Therefore, SPME is proposed as a promising strategy by improving the compatibility of samples with analytical instruments [10,11].

* Corresponding authors.
** Corresponding author at: CAS Key Laboratory of Biobased Materials, Qingdao Institute of Bioenergy and Bioprocess Technology, Chinese Academy of Sciences, Qingdao 266101, China.
E-mail addresses: fayun@qibebt.ac.cn (Y. Fa), zhaozs@qdu.edu.cn (Z. Zhao), yuyl@mail.neu.edu.cn (Y. Yu).

https://doi.org/10.1016/j.cclet.2021.10.030
1001-8417/

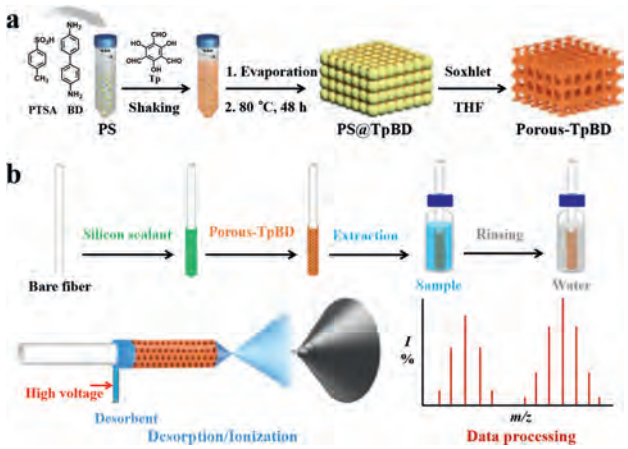

Fig. 1. (a) Schematic illustration of the preparation of Porous-TpBD. (b) Schematic fabrication process of Porous-TpBD coated SPME fiber and subsequent procedure for analysis of TBBPA analogs by SPME coupled with CFDI-MS.

Ambient mass spectrometry (AMS) as a newly developing class of mass spectrometry technology is proposed for environmental analysis, because it can perform real-time, direct, rapid and high-throughput analysis of target compounds in samples with minimal (or without) sample preparation under open and ordinary conditions [12]. The "ambient innovation" of MS technology opens up novel possibility for the development and application of SPME [13]. SPME coupled with AMS (SPME-AMS) possesses obvious superiorities, *e.g.*, reducing matrix effects, improving detection sensitivity, increasing detection throughput [14,15]. Developments of adsorbent coatings with high enrichment efficiency and selectivity play an important role in expanding application of SPME-AMS technology to environmental and toxicological studies [8].

Covalent organic frameworks (COFs) as a newly developing crystalline polymer, in which dynamic covalent bond is formed by organic units made of light elements [16–18], are supposed to be an ideal adsorbent with high efficiency for diverse compounds [19]. Since COFs usually possess high thermal and chemical stability, high specific surface area, ultralow density and rich functional groups [20], they become a great choice for adsorbent/coating-based sample preparation technologies, including solid phase extraction (SPE), SPME, *etc.* [21]. Up to present, most of the reported COFs are microporous and small mesopore structures, generally slowing down the mass transfer and limiting the accessibility of macromolecules to their inner surface [22]. Hence, it is essential to open up an effective avenue to introduce larger pores (mesopores and/or macropores) into microporous COFs to construct hierarchical porous structure, promoting the mass transfer rate and increasing more active sites [22,23].

Herein, hierarchical porous COFs (Porous-TpBD) are synthesized by a polystyrene spheres (PS) template-assisted method, and used to construct SPME coatings by a direct-coating method. The SPME fiber is directly immersed into aqueous solutions to extract TBBPA analogs (Table S1 in Supporting information). Afterwards, TBBPA analogs are effectively desorbed and detected by constant flow desorption ionization-mass spectrometry (CFDI-MS) without chromatographic separation process (Fig. 1).

The strong peak at 3.3° (2θ) in the powder X-ray diffraction (PXRD) pattern corresponds to the (100) plane reflection (Fig. S1a in Supporting information). It is very similar to conventional TpBD and simulated TpBD, indicating that the crystal structure of Porous-TpBD remains unchanged after the removal of the PS template [24]. Besides, the broad peak at 19° (2θ) for PS@TpBD could be ascribed to the amorphous PS, corresponding to the disappearance in Porous-TpBD with PS template removal. In the FT-IR spectra of prepared materials (Fig. S1b in Supporting information), typical stretching band peaks at ~3000 and ~700/cm correspond to C–H and monosubstituted aromatic group of the PS [25]. The typical stretching band peaks of conventional TpBD at 1598, 1576, 1453 and 1294 cm^{-1} belong to C=O, C=C, Ar C=C and C–N, respectively [24,26]. PS@TpBD composite combines the characteristic peaks of both PS and TpBD. The disappearance of PS characteristic peak in Porous-TpBD could be attributed to PS complete removal. Thermogravimetric analysis (TGA) presents that Porous-TpBD has favorable heat stability at temperatures below 350 °C (Fig. S2 in Supporting information).

The specific surface area and porosity of conventional TpBD and Porous-TpBD were tested by N_2 sorption isotherms (Fig. S1c in Supporting information). The conventional TpBD shows a typical type I isotherm, increasing sharply at low relative pressure, and suggesting the microporosity of COFs. The characteristic is also confirmed by the corresponding pore size distribution curve (Fig. S1d in Supporting information). For Porous-TpBD, the type I isotherm has a significantly increased N_2 adsorption at higher relative pressure, indicating that the additional macroporosity is successfully introduced with the assistance of PS template. Meanwhile, mesopores are also observed in the pore size distribution (Fig. S1d). The Brunauer-Emmett-Teller (BET) surface area and total pore volume of Porous-TpBD (797 m^2/g, 0.75 cm^3/g) are higher than those of conventional TpBD (638 m^2/g, 0.41 cm^3/g), corresponding to the formation of porous structures.

The morphological features were characterized by scanning electron microscopy (SEM). PS plates with a homogeneous size and an average diameter of ~500 nm (Fig. S1e in Supporting information). The PS@TpBD composites exhibit TpBD coated on the surface of a pile of tightly packed PS nanoparticles (Fig. S1f in Supporting information). After Soxhlet extraction with tetrahydrofuran, Porous-TpBD predicably consists of porous structures (Fig. S1g in Supporting information). In contrary, the conventional TpBD synthesized in the absence of PS template features bulk particles (Fig. S1h in Supporting information). Ultimately, coated SPME fiber was prepared by the direct coating method [27,28]. The top view (Figs. S1i, j in Supporting information) and cross-section (Figs. S1k, l in Supporting information) SEM images of SPME fiber display uniform coverage of Porous-TpBD, with the thickness of Porous-TpBD coating at ~20 μm. The conventional TpBD-coated SPME fiber shows almost the same coating thickness as Porous-TpBD based SPME fiber (Fig. S3 in Supporting information), indicating that their extraction efficiency has comparability.

The methanol solution containing internal standard $^{13}C_{12}$-TBBPA and TBBPA analogs (100 μg/L) was used as an electrospray reagent, and analyzed by direct injection electrospray ionization mass spectrometry (ESI-MS) to get MS testing conditions (Fig. S4, Table S2 in Supporting information). The extraction ability of Porous-TpBD toward TBBPA analogs was assessed through Porous-TpBD based SPME coupled with CFDI-MS (Fig. 1b). As shown in Fig. 2, the extraction capability of Porous-TpBD is 2.3–3.6 times than conventional TpBD, far better than commercial coatings (5.7–26.3 times than polydimethylsiloxane/divinylbenzene (PDMS/DVB), polyacrylate (PA) and PDMS). The higher extraction capability should be attributed to the integration of multiple porous structures (microporous, mesoporous and macroporous) and the natural features of conventional TpBD (*i.e.*, strong π-π, hydrophobic interactions with TBBPA analogs [29]), promoting the diffusion/mass transfer and improving the approachability of TBBPA analogs to the inner surface [22,30]. The natural properties of the micropores (diameter ~1.3–2.0 nm) are sufficient to accommodate TBBPA analog molecules (Fig. S5 in Supporting information), and the enhanced π-π interaction facilitates the adsorption of TBBPA analogs on the inner surface of the Porous-TpBD. Beyond that, the hydrophobic interactions between the hydrophobic property of TBBPA

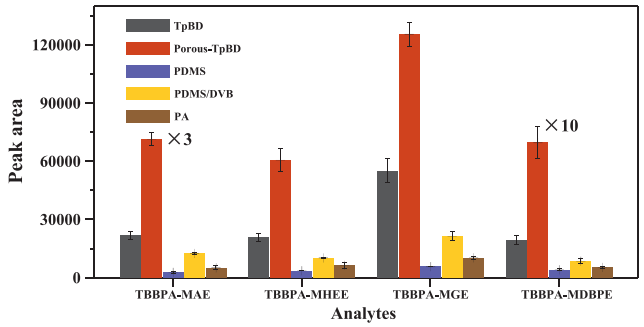

Fig. 2. Comparison of extraction ability of different SPME coatings. The concentration of TBBPA analogs was 1 μg/L.

analogs (logK_{ow} of TBBPA-MAE, TBBPA-MHEE, TBBPA-MGE, and TBBPA-MDBPE are 8.61, 6.79, 7.30 and 9.36, respectively) [31] and Porous-TpBD with a hydrophobic skeleton is another important contributing factor [32].

As the mineral salt often presents negative impacts on determination results [33–35]. Here, it was examined by adding NaCl (0–2000 mmol/L) to TBBPA analog solutions. No obvious interference has been observed when the NaCl concentration is less than 1000 mmol/L (Fig. 3), and far superior to poly(methacrylic acid-*co*-ethylene dimethacrylate-*co*-single wall carbon nanotubes) (poly(MAA-EDMA-SWNT)) monolith coating (20 mmol/L of NaCl) [36] and poly(MMA-EDMA-*co*-multi-wall carbon nanotubes) (poly(MAA-EDMA-MWNT)) monolith coating (40 mmol/L of NaCl) [37], suggesting that the developed Porous-TpBD based SPME-CFDI-MS is conducive to the direct analysis of saline water samples.

The total ion chromatogram (TIC, Fig. S6 in Supporting information) and extracted ion chronograms (EIC, Fig. 4) of the quantitative ions of TBBPA analogs and internal standard $^{13}C_{12}$-TBBPA show that the entire mass spectrometry procedure can be completed in 2.0 min. The calibration curves of concentration and peak area ratio show that except for TBBPA-MDBPE, the linear range is

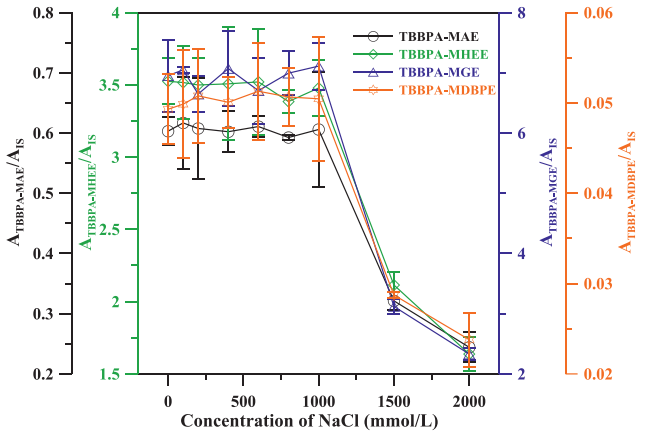

Fig. 3. Salinity tolerance of the Porous-TpBD based SPME-CFDI-MS for detection of TBBPA analogs. The working solutions contain 1 μg/L TBBPA analogs and $^{13}C_{12}$-TBBPA.

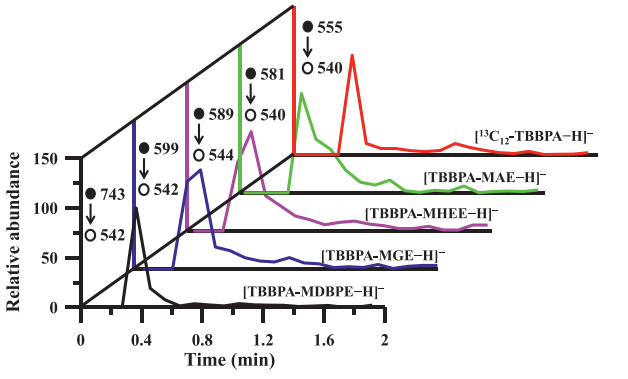

Fig. 4. Extracted ion chronograms (EIC) of the quantitative ions of 1 μg/L $^{13}C_{12}$-TBBPA (internal standard) and 1 μg/L TBBPA analogs in deionized water.

Table 1
Application of the Porous-TpBD-coated fiber for preconcentration and analysis of TBBPA analogs in real samples.

Matrix	Analytes	Found (μg/L)[a]	Spiked (0.1 μg/L)		Spiked (1 μg/L)	
			Measured (μg/L)[a]	Recovery (%)	Measured (μg/L)[a]	Recovery (%)
River water 1	TBBPA-MAE	0.051 ± 0.001	0.152 ± 0.003	101	1.009 ± 0.048	96
	TBBPA-MHEE	0.011 ± 0.001	0.113 ± 0.005	102	1.042 ± 0.102	103
	TBBPA-MGE	N.D.[b]	0.102 ± 0.004	102	1.004 ± 0.064	100
	TBBPA-MDBPE	0.033 ± 0.001	0.132 ± 0.004	99	1.013 ± 0.078	98
River water 2	TBBPA-MAE	0.016 ± 0.001	0.116 ± 0.009	100	0.981 ± 0.035	96
	TBBPA-MHEE	0.015 ± 0.002	0.115 ± 0.002	100	0.989 ± 0.012	97
	TBBPA-MGE	N.D.[b]	0.104 ± 0.008	104	1.01 ± 0.051	101
	TBBPA-MDBPE	0.016 ± 0.003	0.118 ± 0.004	102	1.013 ± 0.071	100
River water 3	TBBPA-MAE	0.016 ± 0.001	0.116 ± 0.005	100	0.99 ± 0.036	97
	TBBPA-MHEE	0.029 ± 0.004	0.131 ± 0.002	102	1.042 ± 0.033	101
	TBBPA-MGE	0.005 ± 0.001	0.102 ± 0.001	97	1.022 ± 0.012	102
	TBBPA-MDBPE	0.042 ± 0.003	0.144 ± 0.013	102	1.098 ± 0.14	106
Sea water 1	TBBPA-MAE	0.042 ± 0.002	0.139 ± 0.004	97	1.032 ± 0.046	99
	TBBPA-MHEE	0.066 ± 0.005	0.17 ± 0.002	104	1.116 ± 0.096	105
	TBBPA-MGE	0.006 ± 0.001	0.105 ± 0.002	99	1.02 ± 0.039	101
	TBBPA-MDBPE	0.062 ± 0.008	0.163 ± 0.006	101	1.01 ± 0.06	95
Sea water 2	TBBPA-MAE	N.D.[b]	0.105 ± 0.002	105	1.032 ± 0.047	103
	TBBPA-MHEE	N.D.[b]	0.101 ± 0.012	101	0.964 ± 0.007	96
	TBBPA-MGE	N.D.[b]	0.098 ± 0.006	98	1.024 ± 0.017	102
	TBBPA-MDBPE	N.D.[b]	0.101 ± 0.002	101	1.026 ± 0.031	103
Sea water 3	TBBPA-MAE	N.D.[b]	0.099 ± 0.004	99	1.034 ± 0.006	103
	TBBPA-MHEE	0.058 ± 0.003	0.16 ± 0.008	102	1.042 ± 0.085	98
	TBBPA-MGE	N.D.[b]	0.1 ± 0.01	100	1.007 ± 0.085	101
	TBBPA-MDBPE	N.D.[b]	0.101 ± 0.008	101	0.993 ± 0.036	99

[a] Average ± standard deviation (n = 3).
[b] N.D. = not detected.

0.001–10.0 μg/L, while the linear range of TBBPA-MDBPE is 0.005–10.0 μg/L, and the correlation coefficient (R^2) values are 0.9931–0.9995 (Fig. S7 in Supporting information). The detection limit (3 σ/k) and quantification limit (10 σ/k) of this method are 0.1–1 and 0.4–3.2 ng/L for detection of TBBPA analogs in a 1 mL water sample, respectively (Table S2). The reproducibility of SPME for one fiber and fiber to fiber is evaluated with relative standard deviation (RSD) values of 3.4–5.8% ($n = 10$) and 4.0–7.3% ($n = 6$), indicating satisfactory reusability and stability. Compared with direct ESI-MS [36,37], the detection sensitivity of 10 μg/L TBBPA analog increases 170–185 fold by using the present method, suggesting the significantly improved performance. Compared with some previously reported techniques, this method also exhibits the strengthened analytical ability of TBBPA analogs, *e.g.*, decreasing sample consumption, reducing time requirement, and improving detection sensitivity (Table S3 in Supporting information).

The practical application performance of this method was assessed by detecting TBBPA analogs in 3 river water and 3 seawater samples (Table 1). In river water samples, the concentration ranges of TBBPA-MAE, TBBPA-MHEE, TBBPA-MGE and TBBPA-MDBPE are 0.016–0.051 μg/L, 0.011–0.029 μg/L, not detected (N.D.)−0.005 μg/L and 0.016–0.042 μg/L, respectively. Their concentration ranges in sea water samples are N.D.−0.042 μg/L, N.D.−0.066 μg/L, N.D.−0.006 μg/L and N.D.−0.062 μg/L, respectively. These results are further validated through spiked recovery experiment. By adding 0.1 and 1 μg/L of TBBPA analog standard solution in these samples, the calculated recoveries are 97–105% and 96–106%, respectively, proving the acceptable accuracy for routine analysis of these TBBPA analogs in water samples.

In conclusion, a fast and sensitive analytical protocol for the detection of TBBPA analogs has been developed by Porous-TpBD based CFDI-MS. Due to the improvement of the mass diffusion characteristic in porous structure and more accessible active sites, the extraction efficiency of Porous-TpBD is significantly enhanced, when compared with conventional microporous TpBD and commercial coatings. Meanwhile, the proposed method exhibits the enhanced analytical performances in terms of reducing time requirement, decreasing sample consumption, increasing detection sensitivity, and possessing favorable salt-tolerant ability, reusability as well as stability. The successful detection of ultratrace TBBPA analogs in real water samples shows great potential for studying their environmental occurrence, fate, toxicology and health effects.

Declaration of competing interest

The authors declare that they have no known competing financial interests or personal relationships that could have appeared to influence the work reported in this paper.

Acknowledgments

This work is financially supported by the National Natural Science Foundation of China (Nos. 21922402, 21976185) and the Innovation Academy for Green Manufacture, Chinese Academy of Sciences (No. IAGM2020C20).

Supplementary materials

Supplementary material associated with this article can be found, in the online version, at doi:10.1016/j.cclet.2021.10.030.

References

[1] P.O. Darnerud, Environ. Int. 29 (2003) 841–853.
[2] A. Covaci, S. Voorspoels, M.A.E. Abdallah, et al., J. Chromatogr. A 1216 (2009) 346–363.
[3] A. Liu, G. Qu, M. Yu, et al., Environ. Sci. Technol. 50 (2016) 4203–4211.
[4] A. Liu, Z. Zhao, G. Qu, et al., Environ. Pollut. 243 (2018) 1141–1153.
[5] G. Qu, A. Liu, L. Hu, et al., TrAC Trends Anal. Chem. 83 (2016) 14–24.
[6] M. Lorenzo, J. Campo, Y. Picó, TrAC Trends Anal. Chem. 103 (2018) 137–155.
[7] C.L. Arthur, J. Pawliszyn, Anal. Chem. 62 (1990) 2145–2148.
[8] N. Reyes-Garcés, E. Gionfriddo, G.A. Gómez-Ríos, et al., Anal. Chem. 90 (2018) 302–360.
[9] S. Xia, J. Dong, Y. Chen, Y. Wang, X. Chen, Chin. Chem. Lett. 29 (2018) 107–110.
[10] F.A. Hansen, S. Pedersen-Bjergaard, Anal. Chem. 92 (2020) 2–15.
[11] Q.C. Zhang, Y.Y. Cheng, G.K. Li, X.H. Xiao, Chin. Chem. Lett. 26 (2015) 1470–1477.
[12] R.G. Cooks, Z. Ouyang, Z. Takats, J.M. Wiseman, Science 311 (2006) 1566–1570.
[13] J. Deng, Y. Yang, X. Wang, T. Luan, TrAC Trends Anal. Chem. 55 (2014) 55–67.
[14] L. Fang, J. Deng, Y. Yang, et al., TrAC Trends Anal. Chem. 85 (2016) 61–72.
[15] H. Piri-Moghadam, F. Ahmadi, G.A. Gómez-Ríos, et al., Angew. Chem. Int. Ed. 55 (2016) 7510–7514.
[16] X. Chen, K. Geng, R. Liu, et al., Angew. Chem. Int. Ed. 59 (2020) 5050–5091.
[17] Y. Xie, Y. Chen, X. Sun, Y. Wang, Y. Wang, Chin. Chem. Lett. 32 (2021) 2061–2065.
[18] H.Q. Yin, F. Yin, X.B. Yin, Chem. Sci. 10 (2019) 11103–11109.
[19] H.L. Qian, C.X. Yang, W.L. Wang, C. Yang, X.P. Yan, J. Chromatogr. A 1542 (2018) 1–18.
[20] C.S. Diercks, O.M. Yaghi, Science 355 (2017) eaal1585.
[21] X. Kou, L. Tong, S. Huang, et al., TrAC Trends Anal. Chem. 136 (2021) 116182.
[22] X. Zhao, P. Pachfule, S. Li, et al., J. Am. Chem. Soc. 141 (2019) 6623–6630.
[23] H. Chen, Q.H. Li, W. Yan, Z.G. Gu, J. Zhang, Chem. Eng. J. 401 (2020) 126149.
[24] S. Chandra, S. Kandambeth, B.P. Biswal, et al., J. Am. Chem. Soc. 135 (2013) 17853–17861.
[25] H. Hou, L. Zhang, T. Liu, et al., J. Colloid Interface Sci. 529 (2018) 130–138.
[26] Y. Li, C.X. Yang, X.P. Yan, Chem. Commun. 53 (2017) 2511–2514.
[27] J. Zheng, J. Huang, F. Xu, et al., Nanoscale 10 (2018) 5725–5730.
[28] W. Gao, Y. Tian, H. Liu, et al., Anal. Chem. 91 (2019) 772–775.
[29] Q. Liu, M. Cheng, Y. Long, et al., J. Chromatogr. A 1325 (2014) 1–7.
[30] D.M. Kabtamu, Y.N. Wu, F. Li, J. Hazard. Mater. 397 (2020) 122765.
[31] A. Liu, J. Shi, G. Qu, et al., Environ. Sci. Technol. 51 (2017) 5434–5444.
[32] Z.D. Du, Y.Y. Cui, C.X. Yang, X.P. Yan, ACS Appl. Nano Mater. 2 (2019) 1232–1241.
[33] T.L. Constantopoulos, G.S. Jackson, C.G. Enke, J. Am. Soc. Mass Spectrom. 10 (1999) 625–634.
[34] Z. Zhang, C.J. Pulliam, T. Flick, R.G. Cooks, Anal. Chem. 90 (2018) 3856–3862.
[35] M.M. Rahman, K. Chingin, H. Chen, Chem. Commun. 55 (2019) 9188–9191.
[36] X. Wang, X. Li, Z. Li, et al., Anal. Chem. 86 (2014) 4739–4747.
[37] X. Wang, X. Li, Y. Bai, H. Liu, Chem. Commun. 51 (2015) 4615–4618.